The Small-Gap Equations in Rotary Lip Seals

J.C. Heinrich
C.A. Vionnet

Publication CIMNE Nº 42, November 1993

THE UNIVERSITY OF
ARIZONA
TUCSON ARIZONA
College of Engineering and Mines
Department of Aerospace &
Mechanical Engineering

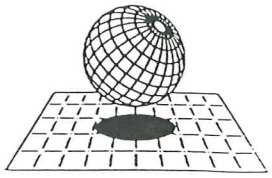

INTERNATIONAL
CENTER
FOR
NUMERICAL METHODS
IN ENGINEERING

The Small-Gap Equations in Rotary Lip Seals

J.C. Heinrich

Aerospace and Mechanical Engineering

University of Arizona

C.A. Vionnet

Aerospace and Mechanical Engineering

University of Arizona

Publication CIMNE Nº 42, November 1993

This report was prepared at the International Center for Numerical Methods in Engineering where the first author is currently on sabbatical leave from the University of Arizona

Centro Internacional de Métodos Numéricos en Ingeniería

Gran Capitán s/n, 08034 Barcelona, España

INDEX

Summary 1

Introduction 1

Analytic Models: The small gap equations in rotary lip seals 2

1. Inner region: Roughness action 3

2. Inner region: Radial oscillation 7

3. Outer region: Centrifugal effect 8

Penalty function formulation for the N-S equations 11

Boundary conditions 12

Finite element method 12

Numerical examples 13

Conclusions 22

References 24

THE SMALL-GAP EQUATIONS IN ROTARY LIP SEALS

Juan C. Heinrich* and Carlos A. Vionnet
Department of Aerospace and Mechanical Engineering
University of Arizona
Tucson, Arizona 85721

SUMMARY

The study of a thin, incompressible Newtonian fluid layer trapped between two almost parallel, sliding surfaces has been actively pursued in the last decades. This subject includes lubrication applications such as slider bearings or the sealing of non-pressurized fluids with rubber rotary shaft seals. In the present work we analyze the flow of lubricant fluid through the micro-gap of rotary lip seals. This study is carried out assuming that a "small-gap" parameter δ attains an extreme value in the Navier-Stokes equations. In particular, the effect of surface roughness, excentricity and centrifugal forces is analyzed using this technique. The precise meaning of small gap is achieved by the particular limit $\delta = 0$ which, within the bounds of the hypotheses, predicts transport of lubricant through the sealed area by centrifugal instabilities. Numerical results obtained with the finite element method are presented.

INTRODUCTION

Radial lip seals are relatively simple elements widely employed in diverse types of rotary machines. This oil resistant elastomeric component is often used to seal rotating shafts at low oil pressures, avoiding the transport of contaminant to, or lubricant from, the rolling bearings system it protects. The seal, bonded through a metallic case to the oil reservoir, is stationary and presents a narrow section that slides over the moving surface of the rotary shaft (Fig. 1).

The lip is designed to have an interference with the shaft. In addition, a garter spring may be used to link both members throughout the lifetime of the seal. Therefore, once the piece is mounted, the compliance of the elastic body ensures a perfect fit between the lip seal and the cylindrical surface of the shaft. Under these conditons, some of the initial seal asperities wear out after a brief period of time, leaving an extremely thin layer of lubricant fluid that separates the seal from the contact surface. This was first noticed by Jagger (1977) and, ever since, numerous explanations attempted to account for two consequences of this experimental fact: the hydrodynamic force able to sustain a gap between the two bodies and the mechanisms that prevents the fluid from leaking through.

Jagger proposed that the surface tension of the sealed fluid controls leakage thanks to a meniscus formed on the air side. Kawahara and Hirabayashi (1977) observed that a properly installed and functional seal leaked when the installation was reversed. But the chosen tool by many researchers to attempt to answer these fundamental questions has been lubrication theory, with the assumption of a relative parallel sliding between two rough surfaces (Hirano et. al. 1961). The load-carrying capacity of parallel sliding of rough surfaces was first studied by Davies (1961). Later on, Jagger and Walker (1966 - 1967) assumed that the asperities of the seal act as micro-bearings pads in

* Currently with the International Center for Numerical Methods in Engineering, Barcelona, Spain.

the contact area. However, Lebeck (1986 a, b) concluded that none of the existing models can fully explain the sliding motion as commonly observed in experiments. Gabelli and Poll (1990) studied the action of the surface microgeometry in the formation of the lubricant film. They found that the contribution of mechanical pressure to the load-carrying capacity due to body contact is very small and indeed negligible. Salant (1990) claimed that micro-ondulations in the lip surface restrict leakage by virtue of a "reverse-pumping" process in which fluid is driven from the low to the high pressure side. However, no one has really observed such micro-ondulations, either in static or dynamic conditions. (Gabelli 1992)

Combinations of angular velocity and shaft eccentricity beyond the ability of the sealing device to maintain contact with the shaft would cause the seal to leak profusely. It has been suggested that an inherent pumping mechanism, sufficient to counterbalance those influences promoting leakage, would be given by the relative motion between the sealing surfaces, Johnston (1989). Besides all these hypotheses, at present there is a wide gap between theory and practice, and a feasible explanation of the mechanisms involved in the sealing action is still pending, even though elastomeric radial lip seals have been used since the 1940's.

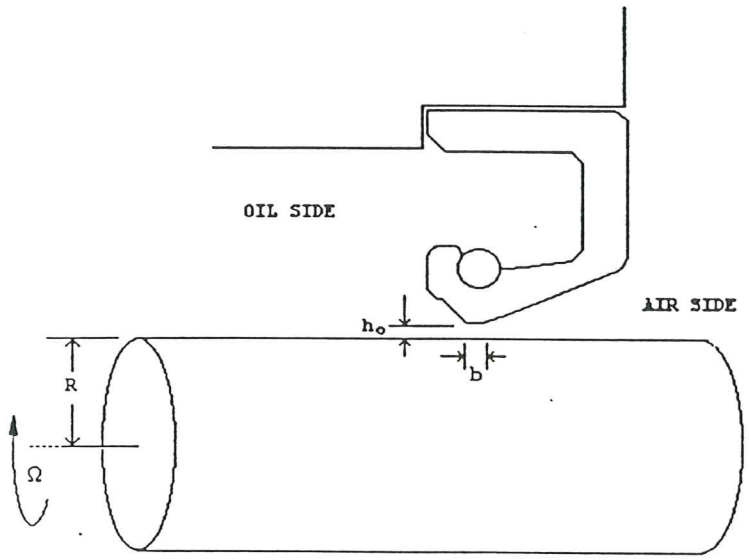

Fig. 1 - Cross section of a typical rubber lip seal

ANALYTIC MODELS: THE SMALL GAP EQUATIONS IN ROTARY LIP SEALS.

We assume an oil-film already formed ignoring any mechanical contact between the seal and the shaft, as well as any elastic distortion of the upper rubber seal. We consider a thin viscous liquid layer bounded above by a seal and below by a perfectly rounded shaft, without including edge effects such as the free surface observed on the air-side. Despite the fact that the film within the gap is very thin, we assume it to be thick enough to conform to a continuum theory. There is no local rupture of the film such as caviation or dry spots in the contact area, and the layer consists of an incompressible Newtonian fluid with constant properties under isothermal conditions.

We begin with the Navier-Stokes equations written in cylindrical coordinates (Batchelor 1967), setting the direction of the line $r = 0$ coincident with the shaft axis.

$$\frac{1}{r}\frac{\partial(ru_r)}{\partial r} + \frac{1}{r}\frac{\partial u_\theta}{\partial \theta} + \frac{\partial u_z}{\partial z} = 0 \tag{1}$$

$$\frac{\partial u_r}{\partial t} + \vec{u}.grad(u_r) - \frac{u_\theta^2}{r} = -\frac{1}{\rho}\frac{\partial p}{\partial r} + \nu\left(\Delta u_r - \frac{2}{r^2}\frac{\partial u_\theta}{\partial \theta} - \frac{u_r}{r^2}\right) \tag{2}$$

$$\frac{\partial u_\theta}{\partial t} + \vec{u}.grad(u_\theta) + \frac{u_r u_\theta}{r} = -\frac{1}{\rho r}\frac{\partial p}{\partial \theta} + \nu\left(\Delta u_\theta + \frac{2}{r^2}\frac{\partial u_\theta}{\partial \theta} - \frac{u_\theta}{r^2}\right) \tag{3}$$

$$\frac{\partial u_z}{\partial t} + \vec{u}.grad(u_z) = -\frac{1}{\rho}\frac{\partial p}{\partial z} + \nu\Delta u_z \tag{4}$$

where

$$\vec{u} = (u_r, u_\theta, u_z), \quad grad = \left(\frac{\partial}{\partial_r}, \frac{1}{r}\frac{\partial}{\partial \theta}, \frac{\partial}{\partial z}\right), \quad \Delta = \frac{1}{r}\frac{\partial}{\partial r}\left(r\frac{\partial}{\partial r}\right) + \frac{1}{r^2}\frac{\partial^2}{\partial \theta^2} + \frac{\partial^2}{\partial z^2}$$

In the absence of a free surface the gravitational body force is expressed as the gradient of a scalar quantity and, therefore, it has been included in the pressure gradient term.

The analysis of the lubricant flow in the contact region involves, roughly speaking, three very different length scales, namely, the radius R of the shaft ($\sim 0.01m$), the much smaller thickness h_0 of the fluid film ($\sim 10\mu m$) and an intermediate length b characterizing the axial extent of the contact region ($\sim 200\mu m$) (as depicted in Fig. 1).

We will consider three different mechanisms that could induce flow through the contact region under dynamic conditions. Namely the surface roughness, shaft excentricity and centrifugal instabilities. The length scales mentioned above will be used to simplify the Navier-Stokes equations in the "small-gap" limit, i. e., when the parameter $\delta = h_0/R$ formally approaches zero.

1. Inner region: roughness action

If the contact area is formed by two flat surfaces, both rigid and in parallel relative motion, the solution of the governing equations is a combination of a Poiseuille and a Couette flow. This is true if we ignore edge effects, as in the lubrication approximation (see e. g. Batchelor 1967) and for a negligible circumferential pressure gradient this flow is stable to small disturbances (Drazin and Reid 1981). However, given the small thickness of the lubricant film, roughness of similar order in the contact area will introduce considerable variations in the fluid layer. In order to analyze this, consider the irregular surface observed in Fig. 2. We enforce 2π periodicity in θ and expand the asperity surface in a double Fourier series of the form

$$h(\theta, z) = h_0 + \sum_{m=1}^{\infty} \sum_{n=1}^{\infty} \hat{a}_{mn} sin(m\theta - \varphi_m)\ cos\left(\frac{n\pi}{b} z\right) \tag{5}$$

For a dominant frequence, and ignoring the initial phase φ_m, a simple representation of the film thickness is given by (Fig. 3).

$$h(\theta, z) = h_0 + a\ sin(m\theta)\ cos(k_n z) \tag{6}$$

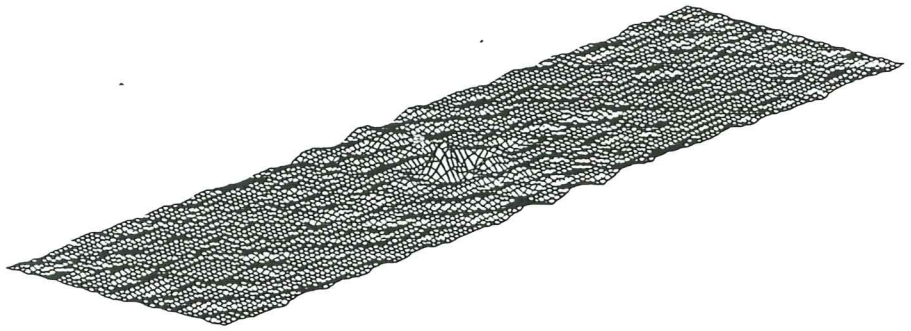

Fig. 2 - Rough contact surface of a lip seal

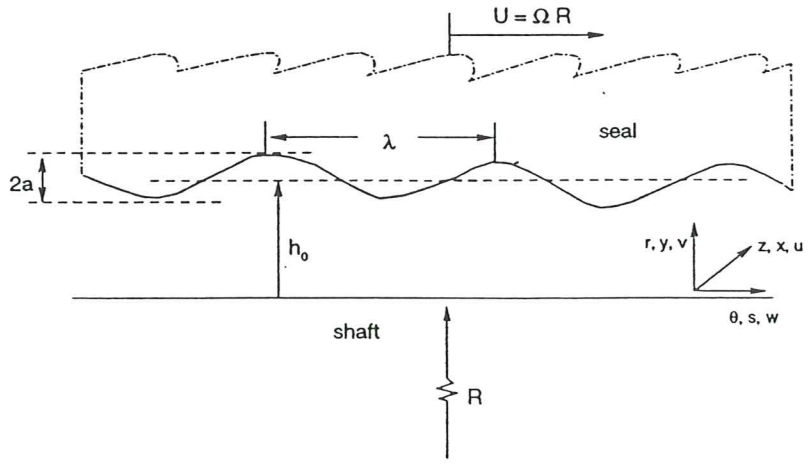

Fig. 3 - Gap between a shaft and a rough seal

where m is an integer, a is an asperity amplitude considered to be small in comparion with h_0 and $k_n = \frac{n\pi}{b}$. Note that $m\theta = \frac{m}{R}(R\theta) = k_m s$, where $k_m = \frac{m}{R} = \frac{2\pi}{\lambda_m}$ is the wave number and $s = R\theta$ is the area lenght coordinate. If we assume parallel sliding motion with the upper surface moving at constant speed U, while the shaft is held stationary, the equation reduces to

$$h(s,z,t) = h_0 + a\ sin[k_m(s - Ut)]\ cos(k_n z) \tag{7}$$

The constant phase velocity can be written as

$$U = \frac{ds}{dt} = \frac{\omega_m}{k_m} \tag{8}$$

where ω_m is the perturbation frequency induced by a roughness of wavelength λ_m. Since $U = \Omega(R + h_0) = \Omega R\left(1 + \frac{h_0}{R}\right) \sim \Omega R$ for $\frac{h_0}{R} \ll 1$, the relationship between the two frequencies ω_m and Ω is

$$\omega_m = \frac{2\pi}{\lambda_m}U = \left(\frac{2\pi R}{\lambda_m}\right)\Omega = m\Omega \tag{9}$$

In addition to the mostly circular Couette flow set by the rotary seal, part of the fluid displaced by an asperity crest will flow axially to the neighboring troughs in response to the incompressible nature of the lubricant. That is, the sliding motion of the upper surface induces alternatively thinning and expansion of the liquid layer that promotes a local flow that scales with $V = \omega_m a$. Therefore

$V = \omega_m a = \frac{2\pi}{\lambda_m}Ua$:scale of velocity in axial plane (r, z)
$U \sim \Omega R$:sliding velocity, scale of velocity in the θ direction

Introducing the dimesionless variables

$$(x,y) = \left(\frac{z}{h_0}, \frac{r - R}{h_0}\right) \qquad \tau = \frac{V}{h_0}t$$

$$(u,v,w) = \left(\frac{u_z}{V}, \frac{u_r}{V}, \frac{u_\theta}{U}\right) \qquad p^* = \frac{(p - p_a)h_0}{\rho\nu V}$$

into the equations of motion, and letting $\delta = \frac{h_0}{R} \to 0$ we get

$$\nabla.\vec{u} = 0 \tag{10}$$

$$R_e^* \, (\partial_\tau + \vec{u}.\nabla)\vec{u} = - \nabla p^* + \nabla^2 \vec{u} \tag{11}$$

$$R_e^* \, (\partial_\tau + \vec{u}.\nabla)w = \nabla^2 w \tag{12}$$

where

$$\vec{u} = (u, v) \quad , \nabla = (\partial_x, \partial_y),$$

$$R_e^* = \frac{2\pi a}{\lambda_m} R_e \quad : \text{Modified Reynolds number}$$

and

$$R_e = \frac{U h_0}{\nu} = \frac{\Omega R h_0}{\nu} \quad : \text{Reynolds number.}$$

Note that the modified Reynolds number contains the four length scales involved in the problem, a, h_0, λ_m and R. Moreover, t was made dimensionless with respect to the inertial time scale $\frac{h_0}{V}$. However, it may be possible to use the viscous time scale $\frac{h_o^2}{\nu}$ so that the time derivative in the acceleration terms would be of order one.

The inertia terms can be neglected if the modified Reynolds number is small, but for $\frac{2\pi a}{\lambda_m}$ of order one, the inertia terms will have a large effect on the velocity and pressure fields for $R_e \geq 1$. This condition can be easily attained with today's low viscosity lubricants and fast rotatory machines, precluding the use of the Reynolds equation. This particular scaling seems to be consistent with the observations of Gabelli and Poll (1990), who found that the average pressure gradient in the circumferential direction is negligible when compared with the pressure gradient across the sealing contact, in agreement with Eq. (12).

The no-slip boundary condition at the upper and lower surfaces are, setting $s = 0$ in Eq.(7) without loss of generality.

$$u = 0, \quad v = 0, \quad w = 0, \quad \text{at } y = 0$$

$$u = 0. \quad v = \frac{dh^*}{d\tau} = -cos\left(\frac{\tau}{\epsilon}\right) \, cos(k_n^* x), \quad w = 1 \quad \text{at} \quad y = 1 - \epsilon \, sin\left(\frac{\tau}{\epsilon}\right) \, cos(k_n^* x)$$

where

$$h^* = \frac{h}{h_0}, \quad k_n^* = \frac{n\pi h_0}{b}, \quad \epsilon = \frac{a}{h_0}$$

This particular set of boundary conditions represents a system of standing waves acting in the axial plane. The small gap limit is equivalent to a postulate of axisymmetric flow, however, it should be noted that the assumption that derivatives with respect to θ are zero is not consistent with the geometry (Fig, 3) except in the limit when $\delta \to 0$. The resulting equations Figs. (10), (11) and (12) show that when $\delta \to 0$ the momentum equations decouple and give a Couette flow in the

θ- direction plus boundary conditions for flow in the axial plane. They clearly show that asperities are unlikely to produce a net flow through the gap under the present assumptions. In the rest of this analysis roughness will be neglected.

2. Inner region: radial oscillation

Consider a rotating seal separated a distance h_0 from the shaft surface and oscillating up and down with frequency Ω and amplitude e (Fig. 4). For a smooth seal rotating at constant angular velocity Ω, the film thickness h can be expressed as

$$h = h_0 + h_r$$

where h_0 is the average separation between seal and shaft and h_r represents the gap displacement induced by radial oscillations of amplitude e. This perturbation provides the simplest model to simulate excentricity of the shaft. The radial displacement becomes

$$h = h_0 + h_r = h_0 + e\ cos(\Omega t) \tag{13}$$

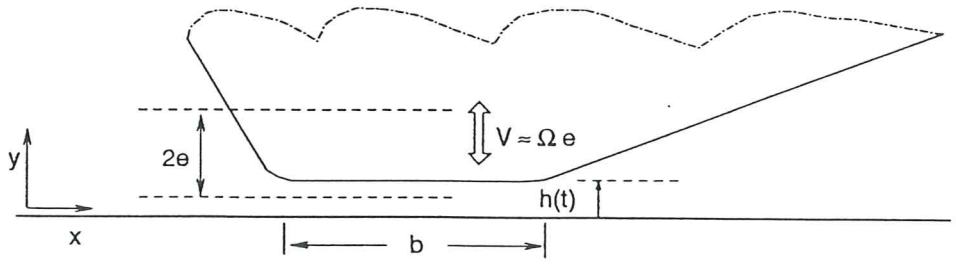

Fig. 4 - Radial oscillations of a rotating seal

A quick computation shows that the ratio between the normal acceleration a_n and the tangential acceleration a_t at any point on the seal is $\sim 0\left(\frac{R}{e}\right)$, which for $R \sim 0.01m$ and $e \sim 10\mu m$ means $\frac{a_n}{a_t} \sim 0(1000)$. In consequence, tangential effects are negligible in comparison with normal variations.

It should be pointed out that frequencies other than Ω are possible for geometric imperfections. Muller and Ott (1984) used a polygon profile in their experiments to generate radial oscillations.

Radial oscillations will have a stronger impact inside the gap than elsewhere since from mass conservation the axial squeezing velocity will be of order $\frac{dh}{dt}\frac{b}{h_0} \sim 0(20 \times \frac{dh}{dt})$ (see Fig. 4).

Introducing the following change of variables, for oscillations of amplitude e of the same order of h_0

$$(x, y) = \left(\frac{z}{h_0}, \frac{r - R}{h_0}\right), \qquad r = \Omega t$$

$$(u, v, w) = \left(\frac{u_z}{\Omega h_0}, \frac{u_r}{\Omega h_0}, \frac{u_\theta}{\Omega R}\right), \qquad p^* = \frac{(p - p_a)}{\rho \nu \Omega}$$

into Eqs. (1) - (4), and letting $\delta = \frac{h_0}{R}$ approach zero, holding other parameters fixed, we get

$$\nabla . \vec{u} = 0 \tag{14}$$

$$\sigma(\partial_\tau + \vec{u}.\nabla)\vec{u} - R_e w^2 \hat{j} = - \nabla p^* + \nabla^2 \vec{u} \tag{15}$$

$$\sigma(\partial_\tau + \vec{u}.\nabla)w = \nabla^2 w \tag{16}$$

where

$$\sigma = \frac{\Omega h_0^2}{\nu} : \text{ squeezing Reynolds number}$$

$$\vec{u} = (u, v), \quad \nabla = (\partial_x, \partial_y), \quad \hat{j} = (0, 1) : \text{ unit vector in radial direction}$$

Several other scalings are possible (Krueger et. al. 1966), but this particular choice seems to be consistent with the Gabelli and Poll observations (Gabelli and Poll 1990). They stated that the average pressure gradient in the circumferential direction is indeed negligible when compared with the pressure gradient across the sealing contact. Ignoring edge effects, this system of equations is subject to the following boundary conditions

$$u = v = w = 0 \qquad \text{at } y = 0$$

$$u = 0, v = -\zeta sin(\tau), w = 1 \qquad \text{at } y = 1 + \zeta cos(\tau)$$

where $\zeta = \frac{e}{h_0}$. The squeezing Reynolds number σ is usually small and inertia terms can be neglected and classical lubrication theory can be applied. Moreover, for small R_e as it turns out to be in most applications, the flow is stable to small disturbances (Drazin and Reid 1981). In the absence of mechanical vibrations, no secondary flow is possible at this level, the circumferential flow is stable and of Couette type.

For small σ and neglecting centrifugal effects, these equations are similar to those governing the squeezing of a thin film between oscillating parallel disks (Hunt 1966). In principle, the flow would be a combination of a pure shearing motion in the azimuthal direction and a squeezing flow in the axial plane.

3. Outer region: centrifugal effect

The changes in the geometry introduce different features in regions located away from the gap. For a slowly-varying channel d = d(z) on the air-side, we rescale the flow field using the nondimensionalization.

$$(x, y) = \left(\frac{z}{d}, \frac{r - R}{d}\right), \qquad \tau = \frac{\nu t}{d^2}$$

$$(u, v, w) = \left(\frac{d}{\nu}u_z, \frac{d}{\nu}u_r, \frac{u_\theta}{U}\right), \qquad p^* = \frac{(p - p_a)d^2}{\rho\nu^2}$$

where d is some mean value of d(z) (see Fig. 5). The equations of motion, Eqs. (1) - (4), in the limit $\delta = \frac{d}{R} \to 0$, become

$$u_x + v_y = 0 \tag{17}$$

$$u_\tau + uu_x + vu_y = -p_x^* + Lu \tag{18}$$

$$v_\tau + uv_x + vv_y - T_a w^2 = -p_y^* + Lv \tag{19}$$

$$w_\tau + uw_x + vw_y = Lw \tag{20}$$

where the subscript denotes differentiation, e. g., $u_x = \frac{\partial u}{\partial x}$. Here

$$T_a = \frac{\Omega^2 R d^3}{\nu^2} \qquad \text{: Taylor number}$$

and

$$L \equiv \frac{\partial^2}{\partial x^2} + \frac{\partial^2}{\partial y^2} \qquad \text{: Laplacian operator in (x, y)}$$

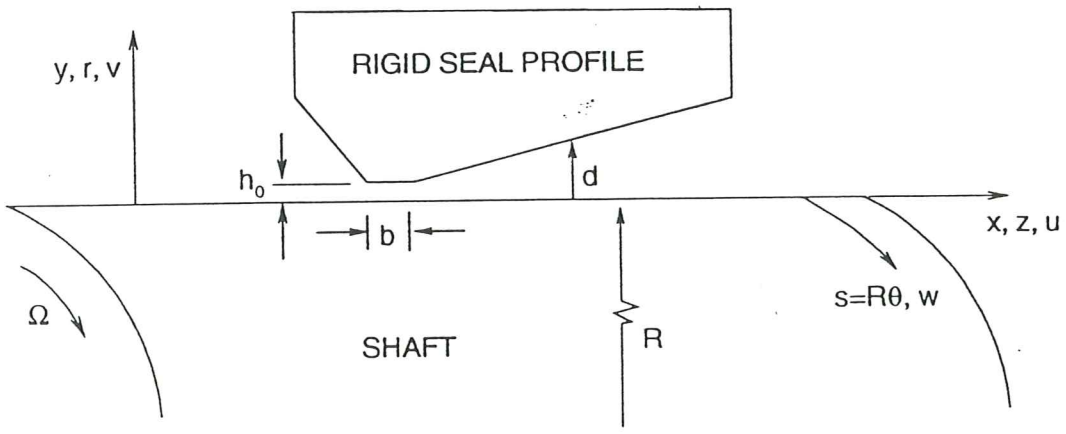

Fig. 5 - Global and local coordinates for centrifugal effects

The above system of equations are the so-called "small-gap" equations, widely used in the context of the stability of Taylor-Couette flows (Hall 1975). While the curvature effects are almost completely neglected, they are retained through the centrifugal term holding the Taylor number fixed as $\delta \to 0$, reflecting the fact that a seal separated from a rotating shaft by a thin lubricating

film is subject to centrifugal instabilities in the vicinity of the contact area. As we will see, this mechanism can produce a significant secondary flow across the gap.

Note that had we used the scaling of section 2 in the inner region, we would have obtained

$$T_a = \frac{\Omega^2 R d^3}{\nu^2} \rightarrow \frac{\Omega^2 R h_0^3}{\nu^2} = \left(\frac{\Omega R h_0}{\nu}\right)^2 \frac{h_0}{R} = R_e^2 \, \delta \rightarrow 0 \text{ as } \delta \rightarrow 0$$

outer region | inner region

and the Taylor number indicates where curvature effects must be retained, regardless of the scales chosen.

The system of Eqs. (17) - (20) is a one-parameter model of axisymetric flow, that can be solved numerically using the finite element method.

PENALTY FUNCTION FORMULATION FOR THE N-S EQUATIONS

In what follows, we denote the coordinte directions as (x, y) or (x_1, x_2), the transverse velocity components as (u, v) or (u_1, u_2), the azimuthal component as w, and the pressure as p; δ_{ij} is the Kronecker delta. For convenience in the treatment of the boundary conditions, we rewrite the equations of motion as

$$\frac{\partial u_i}{\partial x_i} = 0 \tag{21}$$

$$\frac{\partial u_i}{\partial t} + u_j \frac{\partial u_i}{\partial x_j} = T_a w^2 \delta_{i2} + \frac{\partial \sigma_{ij}}{\partial x_j} \tag{22}$$

$$\frac{\partial w}{\partial t} + u_j \frac{\partial w}{\partial x_j} = \frac{\partial^2 w}{\partial x_j \partial x_j} \tag{23}$$

The Taylor number T_a is defined in equation (17), and the stress in the fluid is given by

$$\sigma_{ij} = -p\delta_{ij} + \left(\frac{\partial u_i}{\partial x_j} + \frac{\partial u_j}{\partial x_i} \right)$$

A weak form is obtained by taking the inner product of the transverse momentum equations (22) with a weighting function $\vec{W} = (W_1, W_2)$, and multiplying the azimuthal momentum equation (23) by a scalar function W. The penalty method is implemented introducing the pseudo-constitutive relation (Heinrich and Marshall 1981)

$$p = p_s - \lambda \frac{\partial u_j}{\partial x_j}$$

where p_s is the hydrostatic pressure when the fluid is at rest and λ is the penalty parameter. Upon application of Green's theorem and substituting p by the above expression, we get

$$\int_\Omega \left(\frac{\partial u_i}{\partial t} + u_j \frac{\partial u_i}{\partial x_j} \right) W_i \, d\Omega + \lambda \int_\Omega \frac{\partial u_j}{\partial x_j} \frac{\partial W_i}{\partial x_i} \delta\Omega + \int_\Omega \left(\frac{\partial u_i}{\partial x_j} + \frac{\partial u_j}{\partial x_i} \right) \frac{\partial W_i}{\partial x_j} d\Omega = V_f + S_f \tag{24}$$

$$\int_\Omega \left(\frac{\partial w}{\partial t} + u_j \frac{\partial w}{\partial x_j} \right) d\Omega + \int_\Omega \frac{\partial w}{\partial x_j} \frac{\partial W}{\partial x_j} d\Omega = \int_{\partial\Omega} W \frac{\partial w}{\partial x_j} n_j ds \tag{25}$$

where the surface forces S_f and the volume V_f are defined by

$$S_f = \int_{\partial\Omega} [-pW_i n_i + W_i \left(\frac{\partial u_i}{\partial x_j} + \frac{\partial u_j}{\partial x_i} \right) n_j \,] ds \tag{26}$$

$$V_f = \int_\Omega T_a w^2 \delta_{i2} W_i d\Omega \tag{27}$$

where $\hat{\mathbf{n}} = (n_1, n_2)$ is the unit vector normal to the boundary $\partial\Omega$ and pointing outwards. On a vertical boundary with normal $\hat{\mathbf{n}} = (1, 0)$, the integral of S_f reduces to

$$\vec{W} = (W_1, 0): \qquad -p + 2\frac{\partial u}{\partial x}$$

for normal traction, and

$$\vec{W} = (0, W_2): \qquad \frac{\partial u}{\partial y} + \frac{\partial v}{\partial x}$$

for shear traction, in a weak rather than a pointwise sense.

BOUNDARY CONDITIONS

The boundary conditions are the usual no-slip and no mass penetration at solid walls on the physical boundaries. This is, $u = v = 0$ and $w = 1$ at the lower boundary $y = 0$, which represents the outer surface of the rotating shaft, and $u = v = w = 0$ at the upper boundary, which represents the inner surface of the stationary seal.

At the open boundaries, on both sides of the contact region we apply a free-boundary condition (FBC). We evaluate the line integrals (26) of the weak form of the momentum equations using values computed on the outflow elements. Then, we force the line integrals into the right-hand-side of the discretized equations until convergence is achieved (Papanastasiou et. al. 1992). The natural boundary condition $\partial w/\partial n = 0$ is used in the weak form of the transport equation (25).

FINITE ELEMENTE METHOD

The domain is discretized into M elements and N nodes, we expand the velocity components using biliner isoparametric quadrilateral elements and the pressure with piecewise constant elements. All terms of the weak form of the governing equations are evaluated with full Gaussian integration, except the penalty term, where selective reduced integration is used (Carey and Oden 1986). The weighting functions are set equal to the basis functions, except in the convective terms, where perturbed Petrov-Galerkin functions with balancing tensor diffusivity are employed (Brooks and Hughes 1982; Heinrich and Yu 1988). The time integration is based on the theta method with lumped mass matrices in the time derivatives.

The numerical evaluation of the weighted residuals of the momentum equations leads to a nonlinear system of equations that is solved by a Newton iteration using a direct solver based on Gauss elimination for unsymmetric banded matrices (Dongarra et. al. 1979). A convergence tolerance less than 1% of the relative change $\|\Delta \mathbf{u}^\nu\|/\|\mathbf{u}^\nu\|$ in the velocity field is imposed to terminate each ν-th Newton iteration. The pressure p_e over each element Ω_e is calculated using the weak form

$$p_e = -\frac{\lambda}{\Omega_e} \int_{\Omega_e} \nabla \cdot \vec{u} \, d\Omega \tag{28}$$

where the cross bar denotes reduced integration.

To march in time we use the velocity field $\mathbf{u}^n$ and pressure $\mathbf{p}^n$ at time t_n to evaluate terms of S_f and V_f of the buoyancy force vector $\mathbf{b}^n$. Having determined $\mathbf{b}^n$, we compute the velocity field using the Newton linearization algorithm. Once $\mathbf{u}^{n+1}$ is known, we update the pressure by means of the equation (28) and solve the transport equation for $\mathbf{w}^{n+1}$. The scheme is repeated until steady state is achieved. Time integration is terminated when the relative change between time steps is

$$\left\| \frac{\mathbf{u}^{n+1} - \mathbf{u}^n}{\mathbf{u}^{n+1}} \right\| < \epsilon_1 \quad \text{and} \quad \left\| \frac{\mathbf{w}^{n+1} - \mathbf{w}^n}{\mathbf{w}^{n+1}} \right\| < \epsilon_2$$

where

$$\|\mathrm{a}\|^2 = \sum_j |a_j|^2 \; ;$$

j ranges over the number of degrees of freedom for the particular vector, and ϵ_1 and ϵ_2 are prescribed tolerances. All the following results are obtained with the fully implicit algorithm starting from zero initial conditions.

Numerical examples

The geometry and the finite element mashes employed for the present calculations are shown in Figs. 6, 7 and 8.

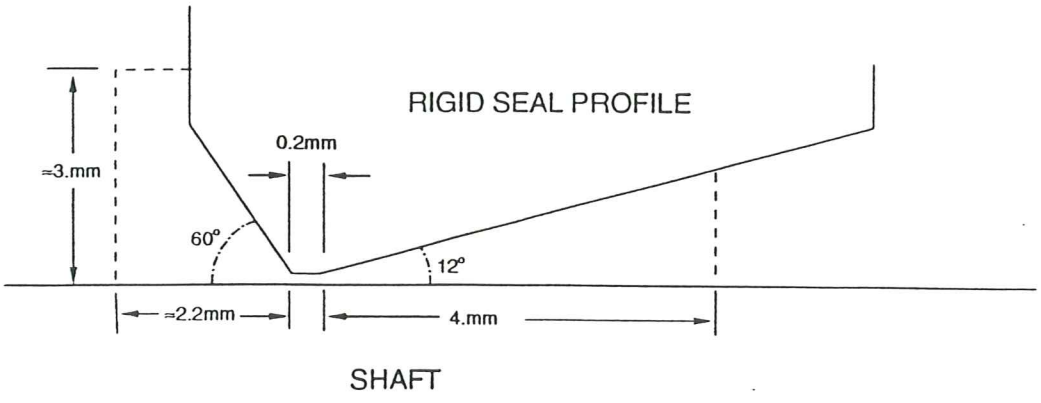

Fig. 6 - Cross section of the seal-shaft configuration

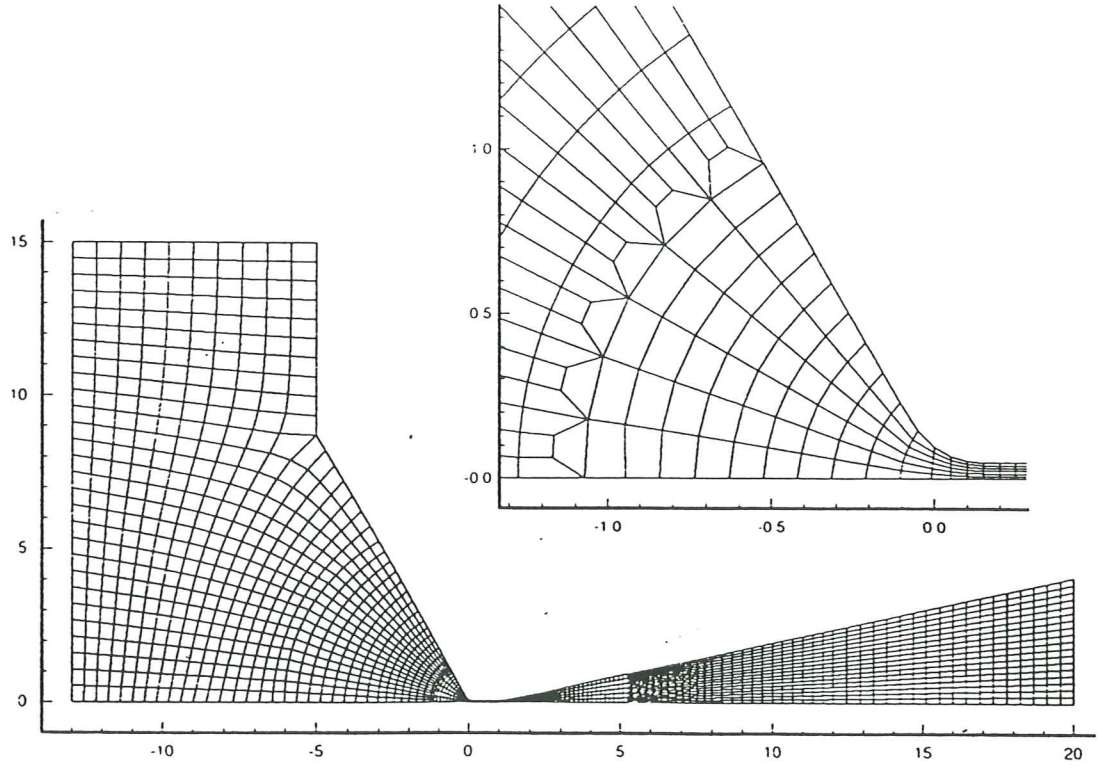

Fig. 7 - Finite element discretization (mesh 1)

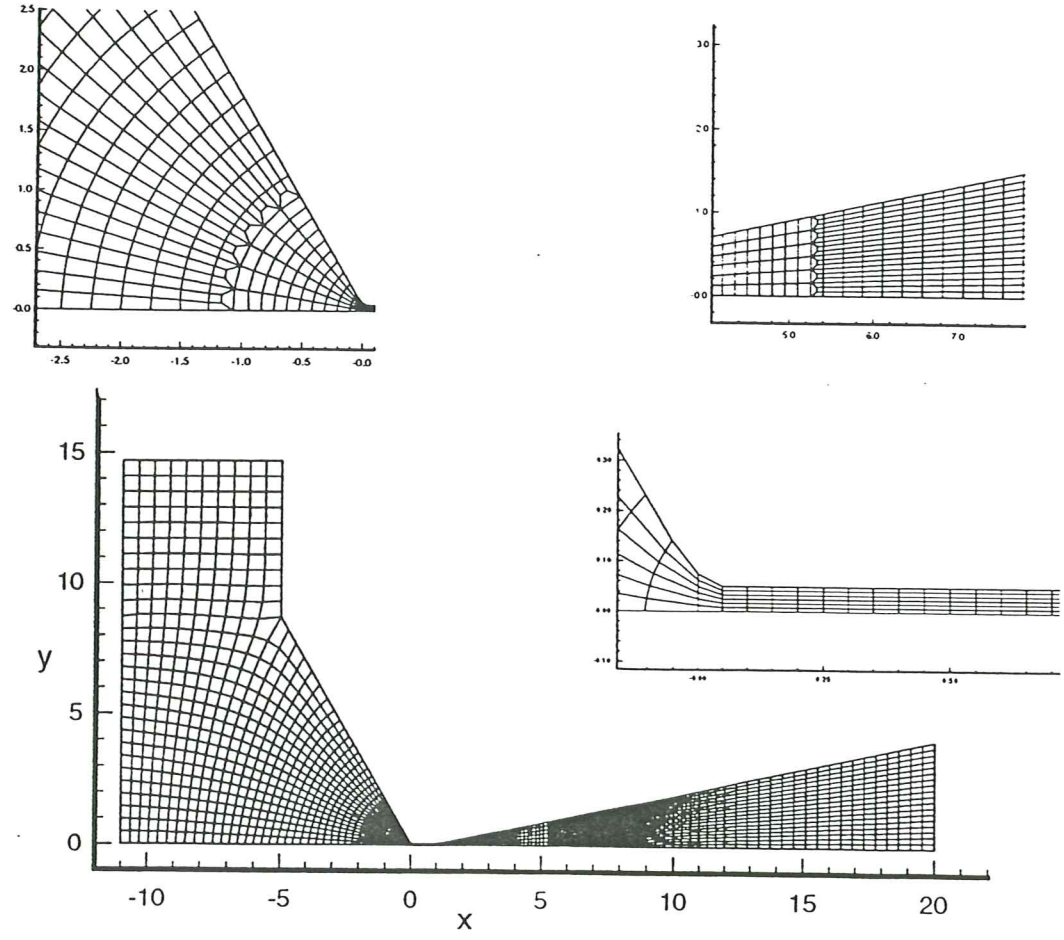

Fig. 8 - Finite element discretization (mesh 2)

The two different discretizations are used to test the influence of the open boundary conditions on the numerical solution. Both meshes contain 2035 nodes and 1864 elements, and the penalty parameter λ is equal to 10^8 in all cases. The dimensions are $h_0 = 10\mu m$ and $b = d = 200\mu m$. The pressure is adjusted at every time step in such a way that it is always zero at the first element, i. e. the element located at $x = -13$, $y = 0$ for the first mesh (Fig. 7), and $x = -11$, $y = 0$ for the second mesh (Fig. 8). Analyses of the time history of the global kinetic energy ensures that steady state is achieved at convergence tolerances $\epsilon_1 = \epsilon_2 = 10^{-4}$.

A series of four steady-state solutions are obtained for values of the parameters $T_a = 2, 5, 10$ and 15. For a lubricatn fluid of kinematic viscosity $\nu = 2.5 \times 10^{-5} \frac{m^2}{s}$, and a shaft radius R = 0.0381 m., these Taylor numbers cover the following range of rotary speed.

Table 1 - Taylor number vs. rotary speed

T_a	$\Omega = \sqrt{\frac{T_a \nu^2}{Rb^3}}$	
	[rad/s]	[rpm]
2	64.0	611
5	101.3	967
10	143.2	1367
15	175.4	1675

First we look at the influence of the domain size on the numerical solutions to determine the effect of the location of the artificial boundaries, especially on the oilside, where the geometry changes abruptly. Volume fluxes, computed with mesh 1 and mesh 2, are tabulated in Table 2.

Table 2

T_a	q - MESH 1	q - MESH 2
2	-0.42×10^{-3}	-0.65×10^{-3}
5	-0.11×10^{-2}	-0.90×10^{-3}
10	-0.21×10^{-2}	-0.15×10^{-2}
15	-0.29×10^{-2}	-0.23×10^{-2}

where the volume flux q across the gap is computed as

$$q = \int_0^{0.05} u \, dy, \qquad x = 0.5$$

Fig. 9 depicts the velocity field computed with both meshes, results are for $T_a = 10$. Plots of both velocity fields are overlapped in Fig. 10 while Fig. 11 shows the overlapped results for the azimuthal component of the velocity and for the pressure.

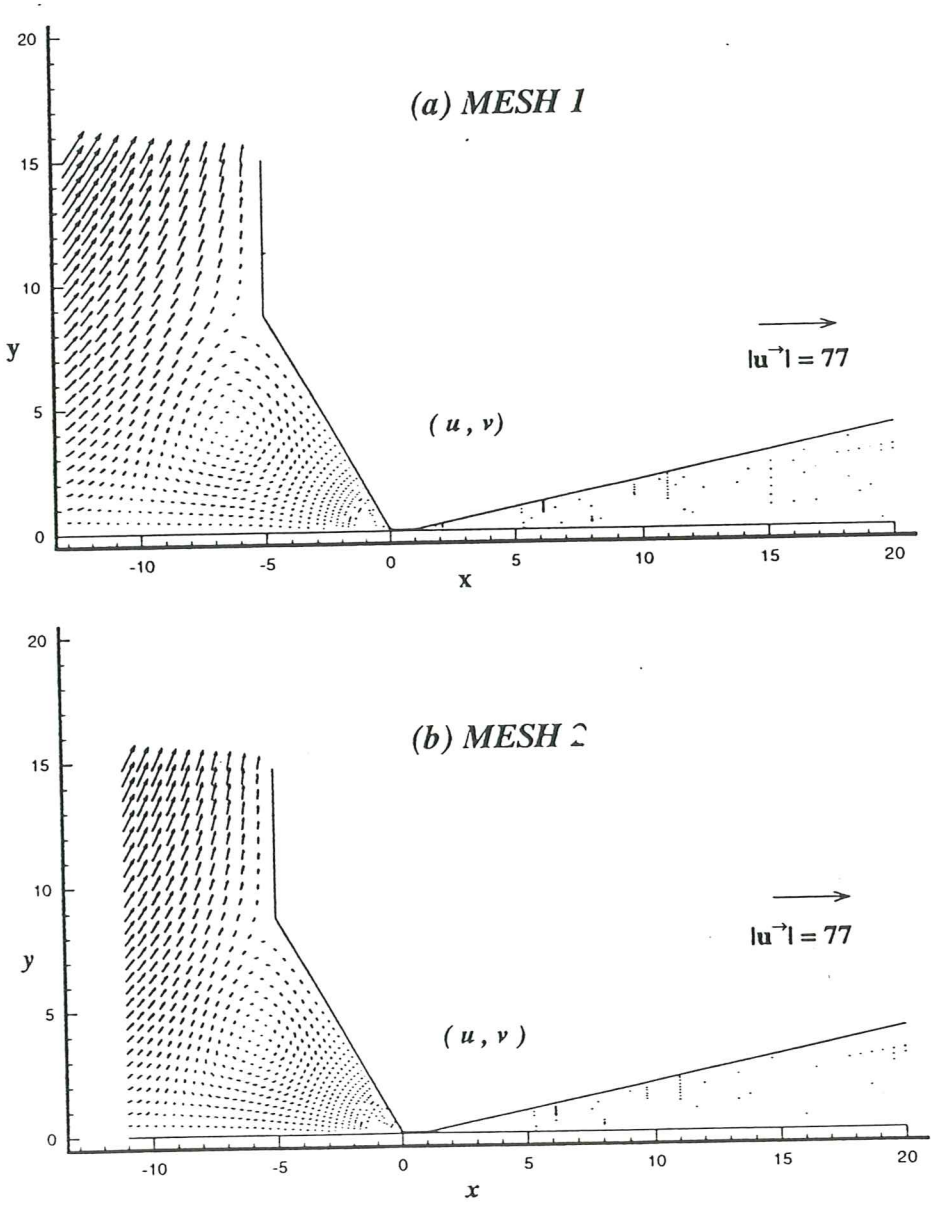

Fig. 9 - Velocity fields obtained with meshes 1 and 2 ($T_a = 10$)

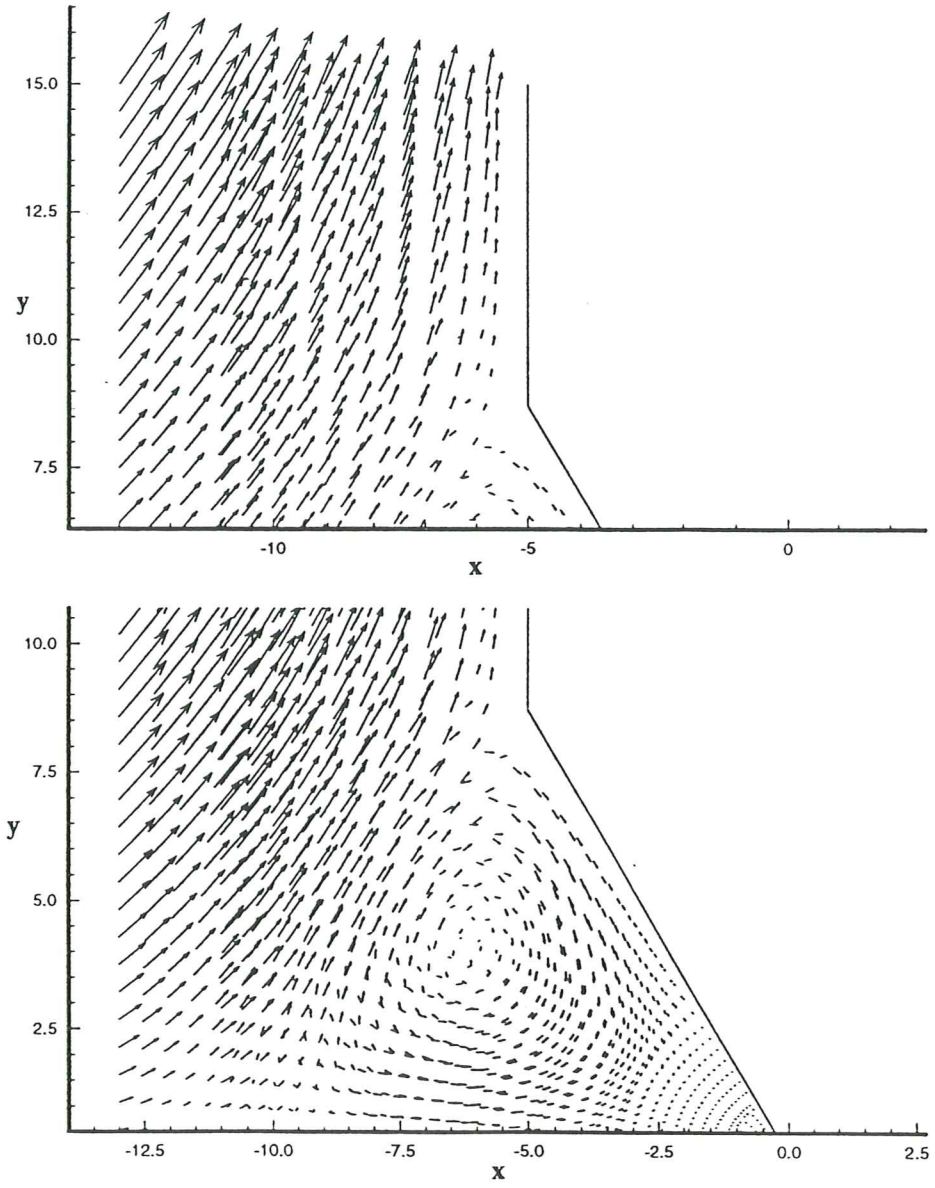

Fig. 10 - Overlapping of the velocity fields plotted in Fig. 9

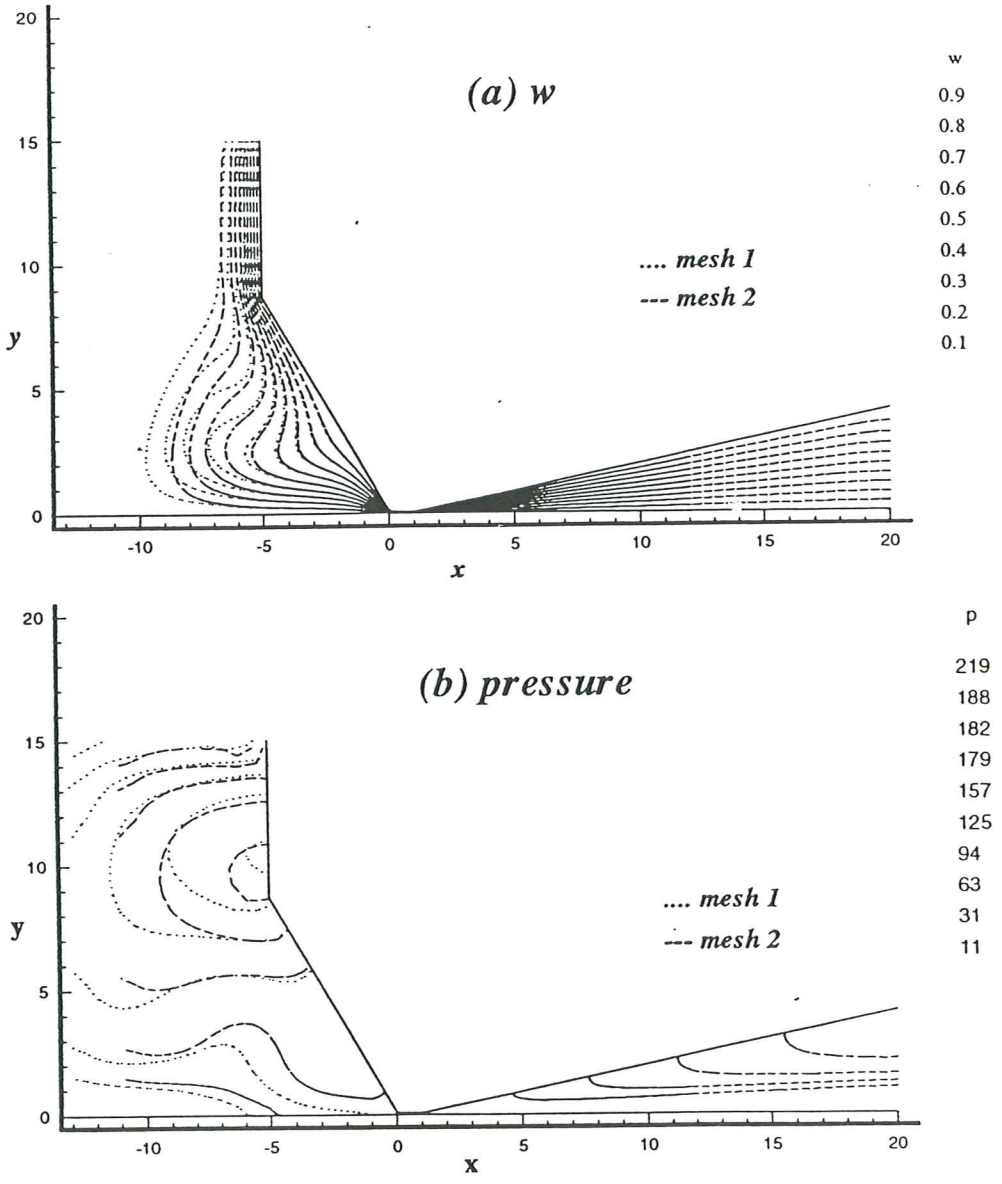

Fig. 11 - Overlapping of numerical results for w and p obtained with meshes 1 and 2

It can be seen that the overall pattern is preserved in both meshes, note that the velocity magnitude shows very large variations over the domain. While a typical order of magnitude for the velocity inside the gap is approximately 0.1, on the oil-side it is of the order of 30. Unfortunately, the gap geometry on its left side is not exactly the same for both meshes, which may have an effect in the above comparison. Figs. 12, 13 and 14 show the transverse velocity field, the circumferential component of the velocity and the pressure, respectively, at $T_a = 15$, using mesh 2.

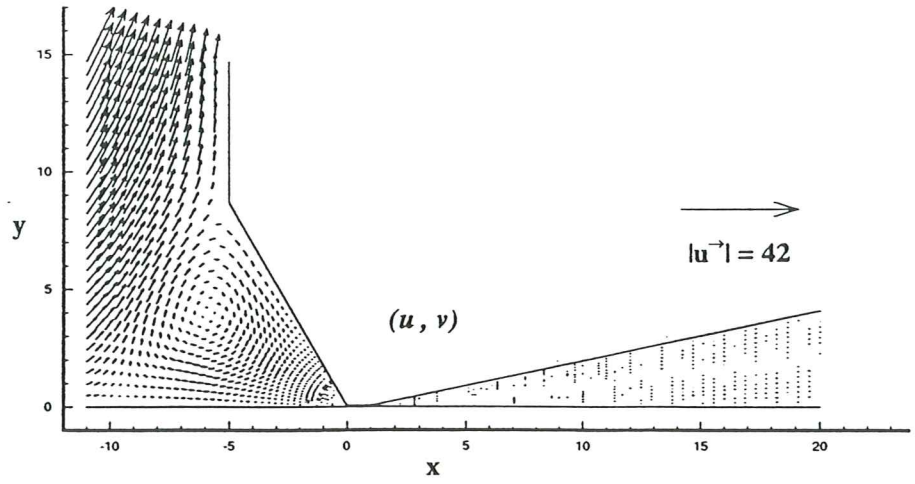

Fig. 12 - Velocity field

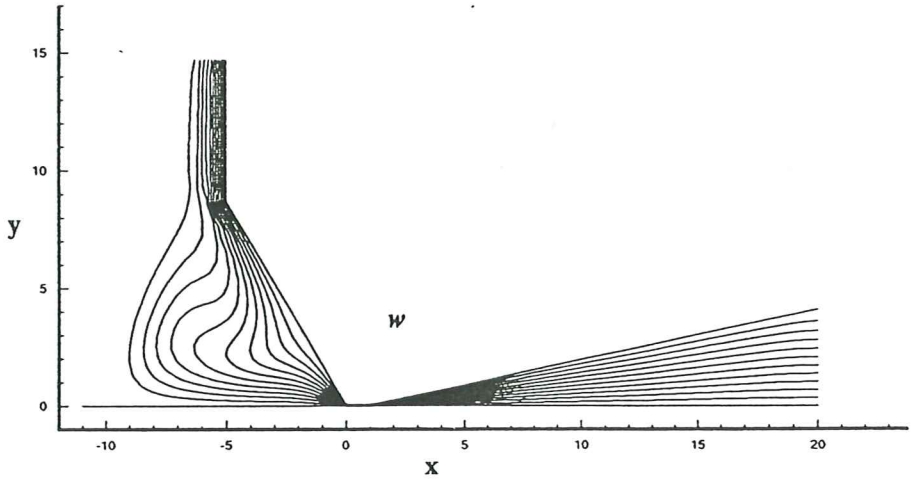

Fig. 13 - Azimuthal component w

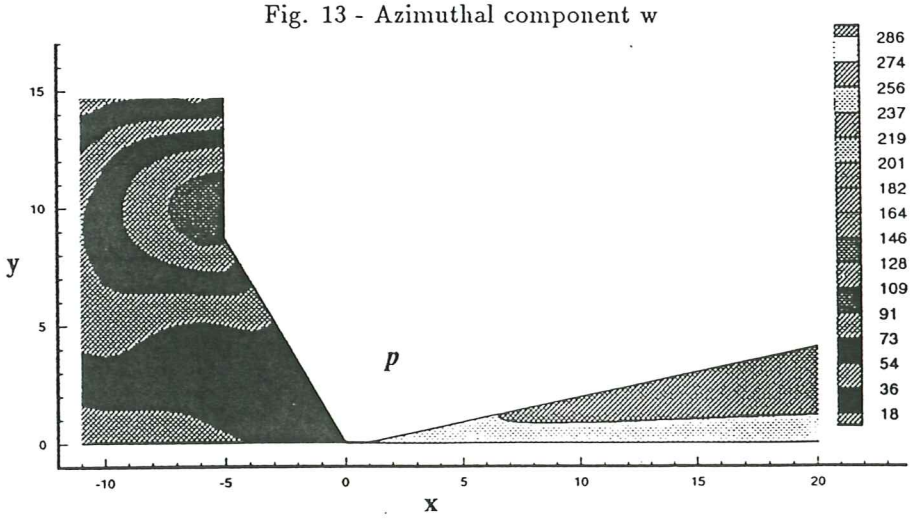

Fig. 14 - pressure

The steep pressure gradient developed along the gap is depicted in Fig. 15, and the resultant volume flux in Fig. 16. Fig. 17 shows the stream function.

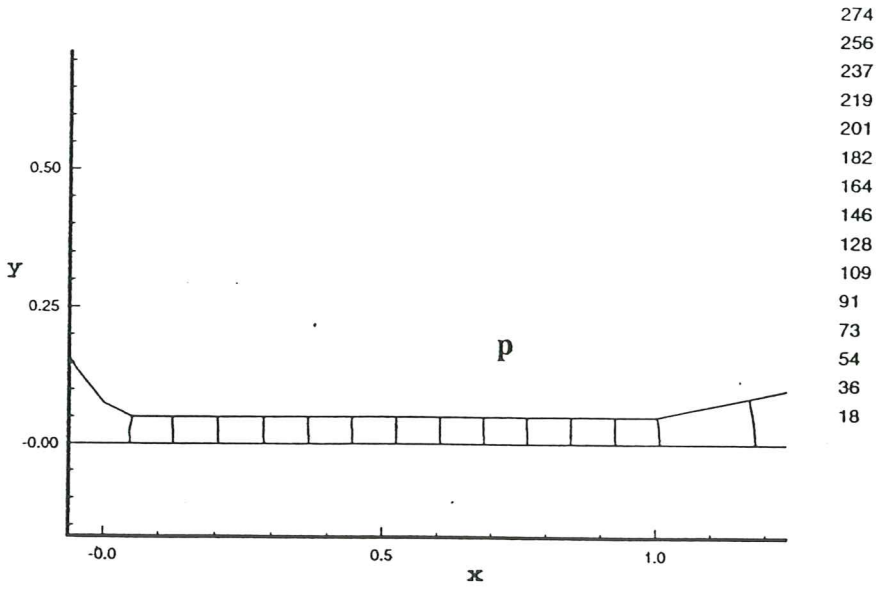

Fig. 15 - Pressure along the gap, $T_a = 15$

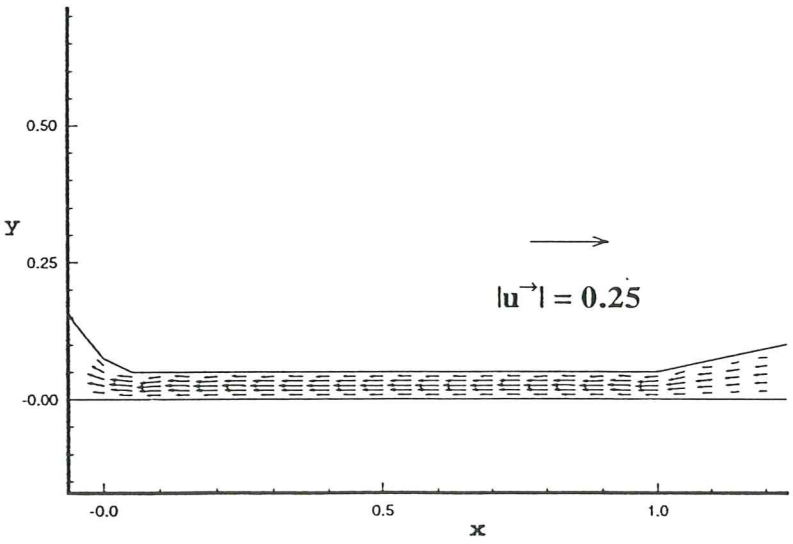

Fig. 16 - Velocity field inside the gap, $T_a = 15$

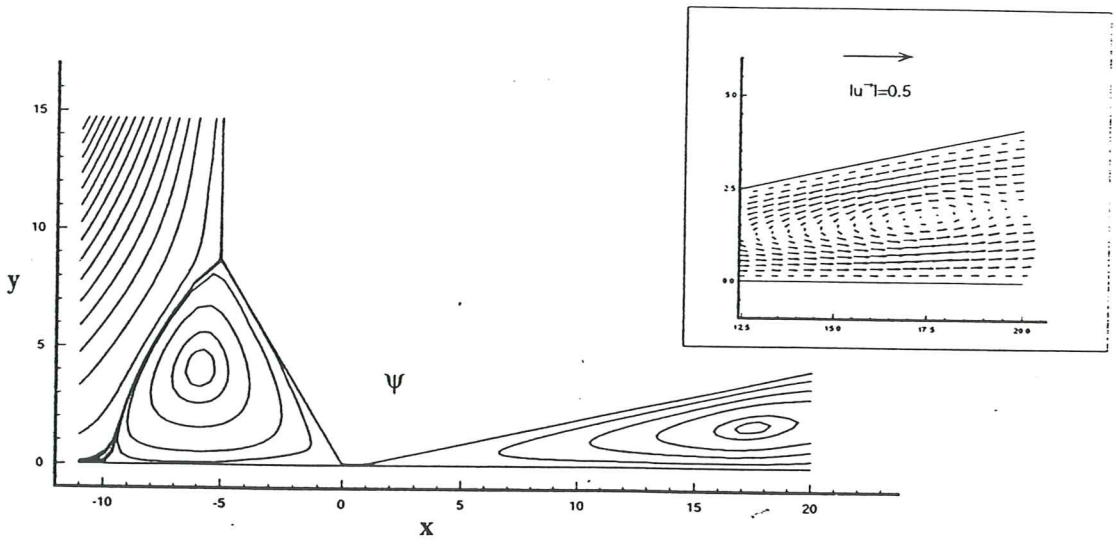

Fig. 17 - Streamline contours, $T_a = 15$

Fig. 18 shows the pressure distribution along the gap for different Taylor numbers. A linear pressure distribution, consistent with the plane Poiseuille flow observed in Fig. 16, is established along the gap where the bounding planes are strictly parallel.

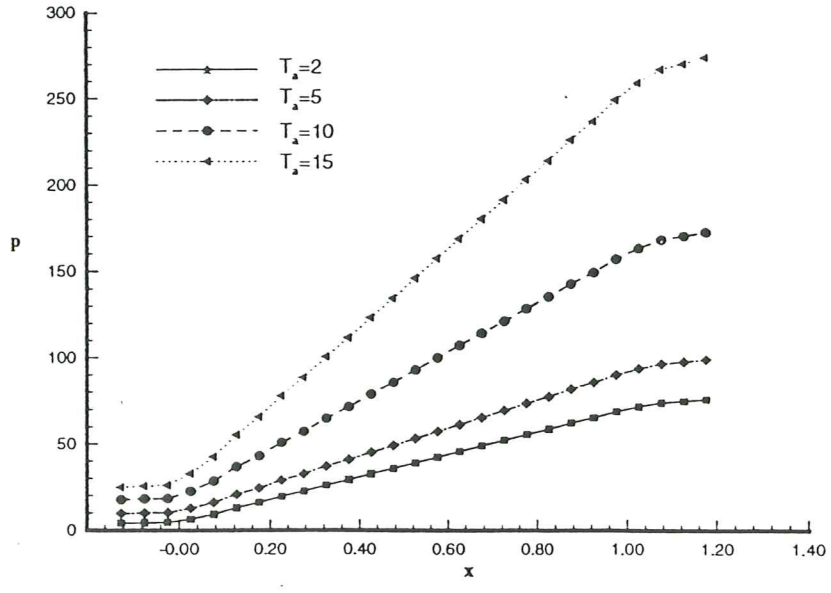

Fig. 18 - Piecewise-constant pressure distribution along the gap

Finally, the presence of large circulation eddies of different strenght on both sides of the gap associated with this pressure jump are depicted in Fig. 19 for $T_a = 10$.

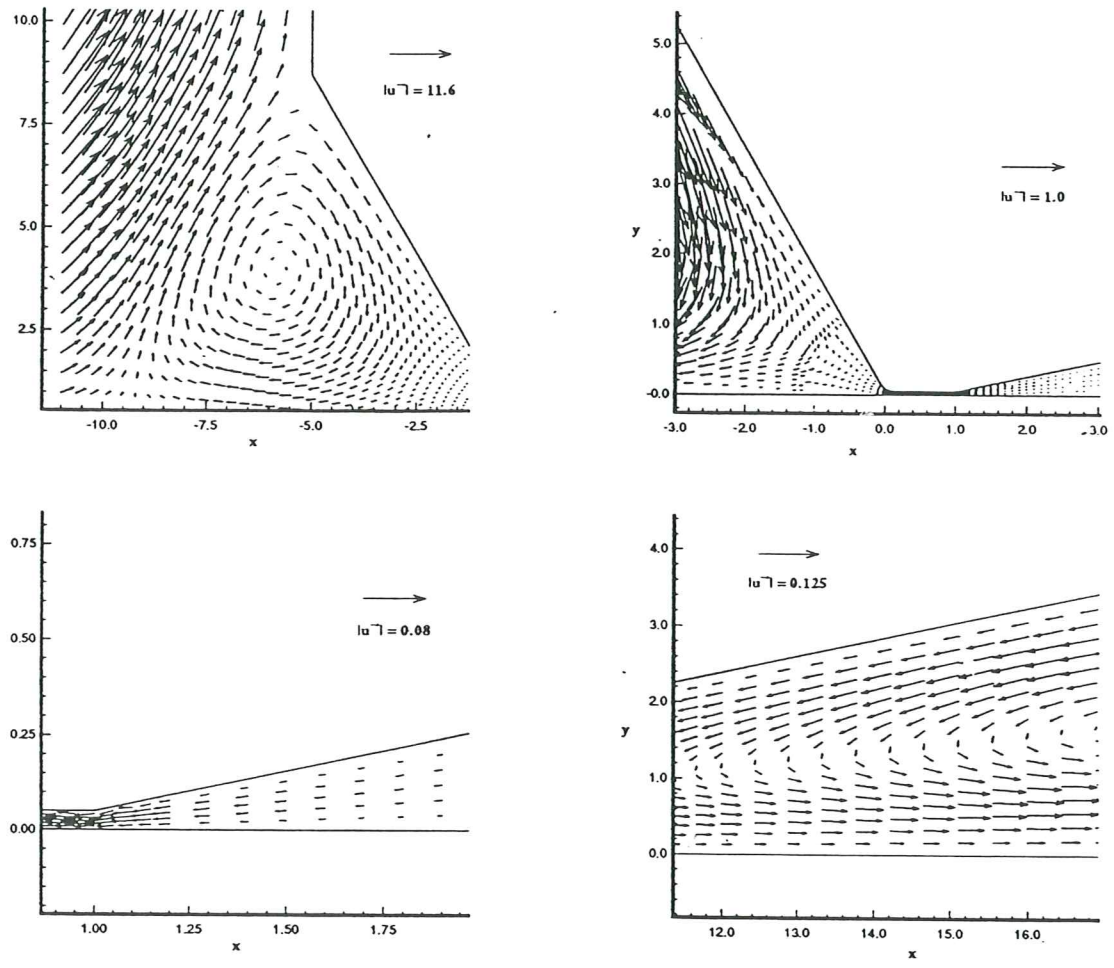

Fig. 19 - Velocity field at different locations $T_a = 10$

CONCLUSIONS

Flow across the microgap in a lip seal has been analyzed starting from the full Navier-Stokes equations and using the relevant length scales to simplify them in order to obtain models that can be more easily interpreted. The basic analytical tool used here has been to take the small gap limit which is particularly relevant to this situation.

Three features of the system have been examined using this technique, the effect of surface roughness, the effect of excentricity and the effect of centrifugal forces. Under the simplified conditions stated in our model we conclude that roughness and excentricity are unlikely to produce flow across the contact region of the seal. On the other hand, centrifugal effects appear to have a strong role in the transport of lubricant under the microgap. The equation obtained using the

limiting process are the well known small-gap equations, used extensively in the context of stability of Taylor-Couette flows. It also has the great advantage that it is amenable to numerical solution, which we have accomplished using the finite element method.

Under the simplified assumptions of this work, the flow under the lip predicted numerically appears to be much stronger than observed in experimental setups. There are at least two clearly identifiable effects that added to the model would make it more realistic and reduce the high flow rates predicted in this work:

1) Capillary effects due to the formation of a meniscus at the oil-air free surface will produce a large pressure drop across the oil-air interface, thus helping to counterbalance the high pressure region developed in the air side.

2) The surface roughness is of the same order as the gap, but has not been taken into account in our calculations. This can be done using a model for flow in a porous medium and will have the effect of reducing the mass flow, due to increased resistance in the medium.

Another important addition to the model in the incorporation of a variable viscosity. Due to temperature variations in the oil within the gap, viscosity may have a large variation across the contact region thus strongly influencing the flow. The addition of the energy equation to the numerical model in order to incorporate thermal effects in the physical properties is currently under development.

REFERENCES

1. Batchelor G.K. (1967) An Introduction to Fluid Dynamics. Cambridge University Press, 1967.

2. Brooks A.N.; and Hughes, T.J.R. (1982) Streamline Upwind/Petrov Galerkin Formulations for Convection Dominated Flows with Particular Emphasis on the Incompressible Navier-Stokes Equations. *Comp. Meth. in Appl. Mech. and Eng.,* Vol. 32, pp. 199-259.

3. Carey G.F.; and Oden, J.T. (1986) Finite Elements. Fluid Mechanics. Vol. VI, Prentice-Hall, Inc.

4. Davies, M.G. (1961) The Generation of Lift by Surfaces Roughness in Radial Face Seals. Int. Conf. on Fluid Sealing. B.H.R.A., Cranfield, England.

5. Dongarra, J.J.; Bunch, J.R.; Moler, C.B.; and Stewart, G.W. (1979) LINPACK User's Guide, SIAM, Philadelphia.

6. Drazin P.G.; and Reid, W.H. (1981) Hydrodynamic Stability. Cambridge University Press.

7. Gabelli A.; and Poll, G. (1990) Formation of Lubricant Film in Rotary Sealing Contacts: Part I - Lubricant Film Modeling. Paper No. 90-Trib-64, ASME/STLE Tribology Conference, Toronto, Canada.

8. Gabelli A. (1992) Private communication.

9. Hall P. (1975) The Stability of Unsteady Cylinder Flows. *J. Fluid Mech.,* Vol. 67, part 1, pp. 29-63.

10. Heinrich, J.C.; and Marshall, R.S. (1981) Viscous Incompressible Flow by a Penalty Function Finite Element Method. *Computer and Fluids*, Vol. 9, pp. 73-83.

11. Heinrich, J.C.; and Yu, C.C. (1988) Finite Element Simulation of Buoyancy-Driven Flows with Emphasis on Natural Convection in a Horizontal Circular Cylinder. *Comp. Meth. Appl. Mech. Eng.,* Vol. 69, pp. 1-27.

12. Hirano, F.; Ishiwata, H.; and Kambayashi, H. (1961) Frictional Sealing Characteristrics of Oil Seals, Proc. 1st Int. Conf. on Fluid Sealing, BHRA, pp. 698-709.

13. Jagger, E.T.; and Walker, P.S. (1966-1967) Further Studies of the Lubrication of Synthetic Rubber Shaft Seals. Proc. Inst. Mech. Engrs. Vol. 181, pp. 101-204.

14. Jagger, E.T. (1957) Study of the Lubrication of Synthetic Rubber Rotary Shaft Seals. Proc. Conf. on Lubrication and Wear. Inst. of Mech. Eng., pp. 409-415.

15. Johnston D.E. (1989) Theoretical Analysis of a Pumping Mechanism Between Relatively Moving Surfaces. Proc. BHRA 12th. Int. Conf. Fluid Sealing, Brighton, UK.

16. Kawahara, Y.; and Hirabayashi, H. (1977) A Study of Sealing Phenomena on Oil Seals. ASLE 77-LL-5B-2.

17. Krueger E.R.; Gross, A.; and Di Prima, R.C. (1966) On the Relative Importance of Taylor-vortex and Non-axisymmetric Modes in Flow Between Rotating Cylinders *J. Fluid Mech.,* Vol. 24, part 3, pp. 521-538.

18. Lebeck A.O. (1986 a) Parallel Sliding Load Support in the Mixed Friction Regime. Part 1. The Experimental Data. ASME *Journal of Tribology,* Vol. 109.

19. Lebeck A.O. (1986 b) Parallel Sliding Load Support in the Mixed Friction Regime. Part 2. Evaluation of the Mechanisms. ASME *Journal of Tribology* , Vol. 109.

20. Leone J.M. (1990) Open Boundary Condition Symposium. Benchmark Solution: Stratified Flow over a Backward-facing Step. *Int. J. Num. Meth. in Fluids* Vol. 11, pp. 969-984.

21. Muller, H.K. and Ott, G.K. (1984) Dynamic Sealing Mechanism of Rubbery Rotary Shaft Seals. Proc. BHRA 10th Int. Conf. Fluid Sealing. Paper K3, Innsbruck, Austria.

22. Papanastasiou, T.C. (1992) Malamataris, N.; and Ellwood, K.: A New Outflow Boundary Condition. *Int. J. Num. Meth. Fluids,* Vol. 14, pp. 587-608.

23. Salant, R.F. (1990) Numerical Analysis of the Flow Field within Lip Seals Containing Microundulations. Paper No. 91-Trib-45, STLE/ASME Tribology Conference, St. Louis, Mo.

24. Stakenborg, M.J.L. (1988) On the Sealing and Lubrication Mechanism of Radial Lip Seals, Diss., Eidenhoven University of Technology.